



The Effect of Annealing Temperatures on Cu₂O Nanoparticle Structural Properties

Karrar A. Alsoltani* 

Department of Physics, College of Education for
Pure Science Ibn-AL-Haitham, University of
Baghdad, Baghdad, Iraq.

Khalid H. Harbbi 

Department of Physics, College of Education for
Pure Science Ibn-AL-Haitham, University of
Baghdad, Baghdad, Iraq.

*Corresponding author: karrar.Ameen1104a@ihcoedu.uobaghdad.edu.iq

Article history: Received 27 November 2022, Accepted 18 January 2023, Published in July 2023.

doi.org/10.30526/36.3.3116

Abstract

In this study, the effect of the annealing temperature on the material properties and the structural properties of cuprous oxide was studied in order to investigate how the annealing temperature affects the material properties, and the temperature varied between 200°C, 300°C, 400°C and 500 °C and was unannealed. The physical properties of the cuprous oxide were measured by X-ray diffraction (XRD). The XRD patterns showed that the Cu₂O nanoparticles were highly pure, crystalline, and nano-sized. From the XRD results, we found the pure cuprite (Cu₂O) phase. The values of crystal size were discovered and calculated by the Halder-Wagner and Size-Strain Plot (SSP) methods, respectively. The crystallite size increased as the annealing temperature increased. As a result, it was discovered that annealing temperature has a significant impact on structural and morphological aspects. In order to calculate physical and microstructural parameters such as internal strain, dislocation density, surface area, and consequently the number of unit cells, the sample was taken into consideration.

keywords: Cu₂O, Originpro, Xrd, halder-wagner, size-strain plot.

1. Introduction

Great importance is given to the preparation of nanoparticles (NPs) and the study of their properties [1]. Their physical and chemical properties attract the current scientific field over bulk materials [2]. Cuprous oxide (Cu₂O) is a p-type transparent semiconductor material with a unit cell containing four oxygen and two copper ions with a cubic structure belonging to the Pn3m space group. The lattice parameters are a, b and c = 4.2696 Å [3]. Many processes have been used for the synthesis of Cu₂O nanostructures. Is currently attracting considerable interest within the fields of both condensed matter physics and materials chemistry. This interest is especially to do with its rich



excitonic structure and potential applications in solar energy conversion, catalysis, sensing, magnetic storage medium, and electrode materials in lithium-ion batteries, etc.[4-5]. In this work nanopowder of Cu₂O with different annealing temperatures Cu₂O powder that has not been annealed as well as powder that has been annealed at 200, 300, 400, and 500°C have been used to explore the impact of annealing temperature on structural characteristics using X-ray diffraction (XRD), and the results have been compared and discussed.

2. Theory

2.1. Method of Halder-Wagner

In the method of Halder-Wagner where Gauss and Lorentzian describe the strain and crystallite size profiles [6].

$$\left(\frac{\beta_{hkl}^*}{d_{hkl}^*}\right)^2 = \left(\frac{1}{D}\right) \left(\frac{\beta_{hkl}^*}{d_{hkl}^*}\right) + \left(\frac{\varepsilon}{2}\right)^2 \quad (1)$$

Where The wavelength of the X-ray plot was $\left(\frac{\beta_{hkl}^*}{d_{hkl}^*}\right)^2$ against $\left(\frac{\beta_{hkl}^*}{d_{hkl}^*}\right)$ is a straight line. where $\beta_{hkl}^* = \beta \cos \theta / \lambda$ and $d_{hkl}^* = 2 \sin \theta / \lambda$. The inverse slope of the line was used to get the mean diameter. The y-intercept yields the strain distortions.[7-8].

2.2. Size-strain Plot Method

The low and medium angle ranges are given more weight in this method, which is advantageous because the overlap between the diffraction peaks is greatly decreased. Now, the relationship between lattice strain and crystal size is provided by [9] using the size-strain plot technique.

$$(d_{hkl} \beta_{hkl} \cos \theta)^2 = \left(\frac{K}{D}\right) (d_{hkl}^2 \beta_{hkl} \cos \theta) + (2\varepsilon)^2 \quad (2)$$

Where $(\beta_{hkl} / d_{hkl})^2$ denotes the X axis and $(\beta_{hkl} / d_{hkl}^2)$ denotes the Y axis. The slope yields the mean crystal size value, and the intersection yields the strain.

3. Results and Discussion

According to the XRD patterns shown in **Figure 1**, the XRD pattern is shown with angles ranging from 10 to 80. Obtained from source <x>, shows in situ for samples 1-5. Through a program (WebPlotDigitizer-4.5), we obtain data for intensity and 2θ of Cu₂O nanoparticles to all profile lines it is possible to index five peaks at $2\theta = 29.78^\circ, 36.56^\circ, 42.39^\circ, 62.51^\circ,$ and 73.46° at the (110), (111), (200), (220) and (311) planes of the cubic phase Cu₂O with a lattice constant of equal 0.4266 nm [10]. These values are very close to those values in International Centre for Diffraction Data JCPDS (PDF, Powder Diffraction File, No. 05-0667, 1996) [10].

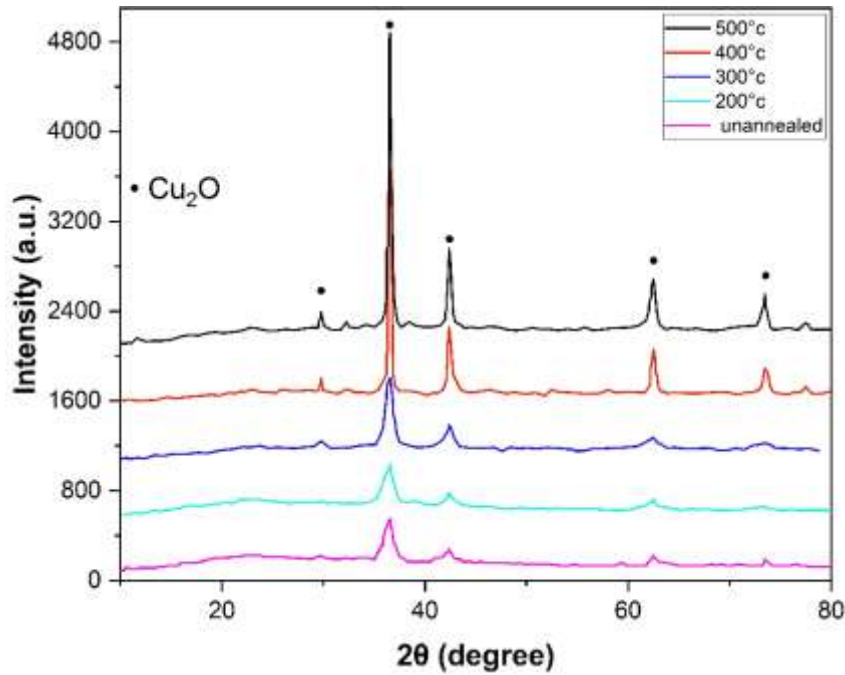


Figure1. XRD patterns of Cu₂O nanoparticles were un and annealed at 200°C, 300°C, 400°C and 500 °C

In addition, this data is used to draw the shape of the peaks using an analytical program (Origin Pro Lab) to calculate the area under the curve and the FWHM is calculated by the program and then calculate integral breadth was the integral breadth which is [11]:

$$\beta = A / I_0 \tag{3}$$

Where A was the area under the curve and the I₀ was the highest intensity of the peak for each sample and for the different peaks respectively.

The below Figures and tables get from an (Origin Pro Lab). These findings will be used to apply the previous equations to compute each crystal's sizes and strains in order to understand how the annealing temperature affects them.

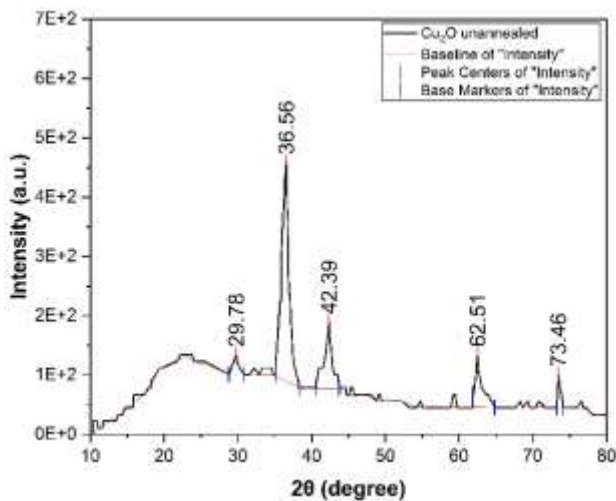


Figure2. XRD patterns of Cu₂O nanoparticles unannealed by Originpro

Table 1. result of Cu₂O NPs unannealed by Originpro

(h k l)	2θ un	Area	FWHM	Height	β
(1 1 0)	29.78	28.64926	0.76338	33.53435	0.854326
(1 1 1)	36.56	437.6825	0.97852	369.031	1.186032
(2 0 0)	42.39	138.7683	0.83286	113.909	1.218239
(2 2 0)	62.51	94.84389	0.75674	88.90931	1.066749
(3 1 1)	73.46	23.95065	0.42235	55.96132	0.427986

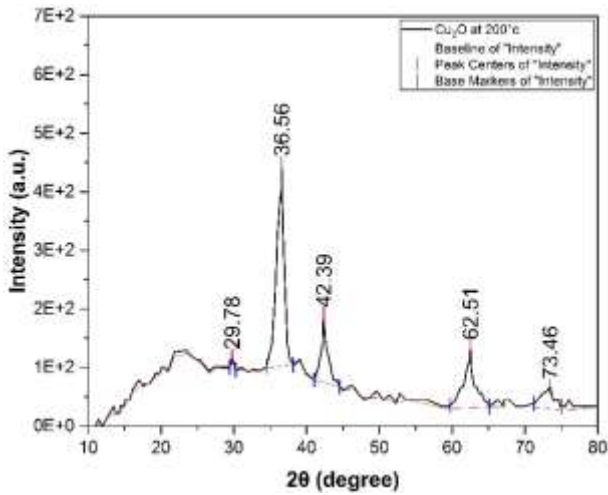


Figure3. XRD patterns of Cu₂O nanoparticles annealed at 200° C by Originpro

Table 2. result of Cu₂O NPs annealed at 200°C by

(h k l)	2θ 200°C	Area	FWHM	Height	β
(1 1 0)	29.78	8.1628	0.1946	20.209	0.4039
(1 1 1)	36.56	403.51	1.0999	345.43	1.1681
(2 0 0)	42.39	117.91	0.6298	115.74	1.0187
(2 2 0)	62.51	175.00	0.9893	103.06	1.698
(3 1 1)	73.46	74.599	1.7634	37.541	1.9871

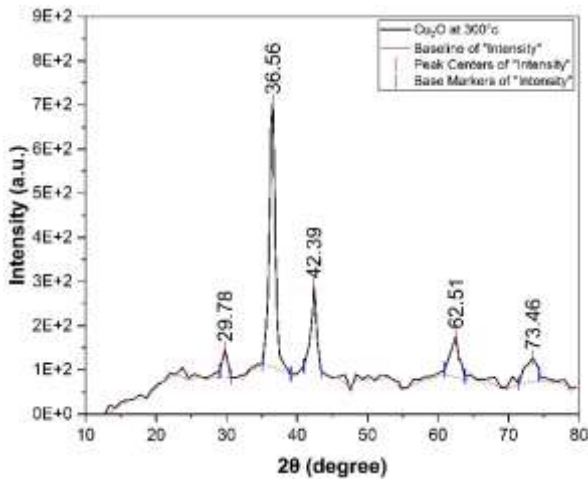


Figure4. XRD patterns of Cu₂O nanoparticles annealed at 300° C by Originpro

Table 3. result of Cu₂O NPs annealed at 300°C by Originpro

(h k l)	2θ 300°C	Area	FWHM	Height	β
(1 1 0)	29.78	56.228	0.4707	63.832	0.8809
(1 1 1)	36.56	611.52	0.8144	601.74	1.0163
(2 0 0)	42.39	212.6	0.8646	203.99	1.0421
(2 2 0)	62.51	134.82	1.2737	92.909	1.4511
(3 1 1)	73.46	103.05	2.2347	53.819	1.9147

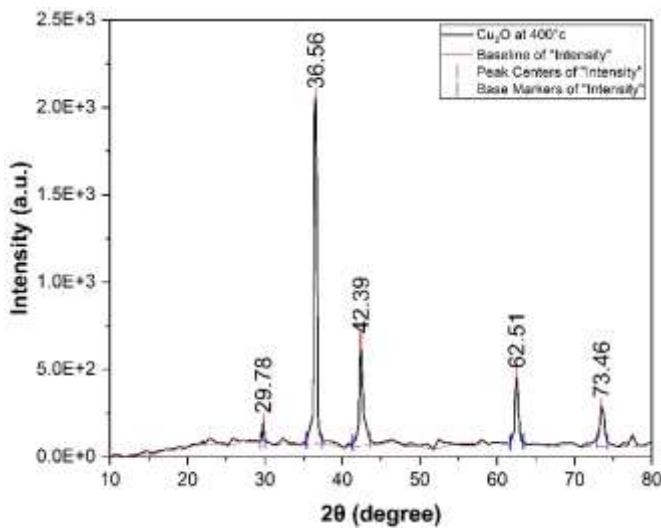


Figure5. XRD patterns of Cu₂O nanoparticles annealed at 400° C by Originpro

Table 4. result of Cu₂O NPs annealed at 400°C by

(h k l)	2θ 400°C	Area	FWHM	Height	β
(1 1 0)	29.78	26.471	0.1204	119.63	0.2213
(1 1 1)	36.56	955.57	0.4433	1985.1	0.4814
(2 0 0)	42.39	386.95	0.4426	598.64	0.6464
(2 2 0)	62.51	222.64	0.5325	386.44	0.5761
(3 1 1)	73.46	168.43	0.6323	231.32	0.7281

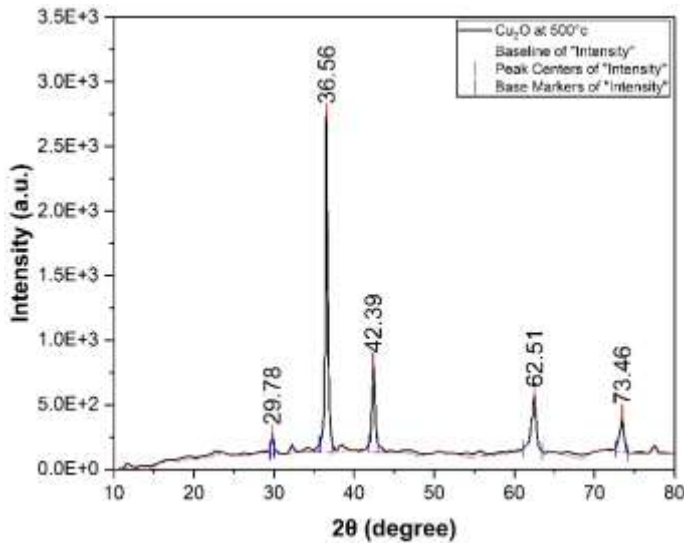


Figure6. XRD patterns of Cu₂O nanoparticles annealed at 500°C by Originpro

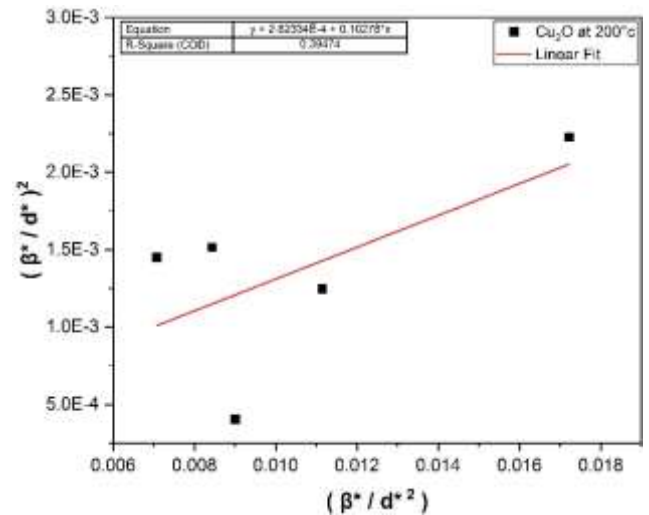
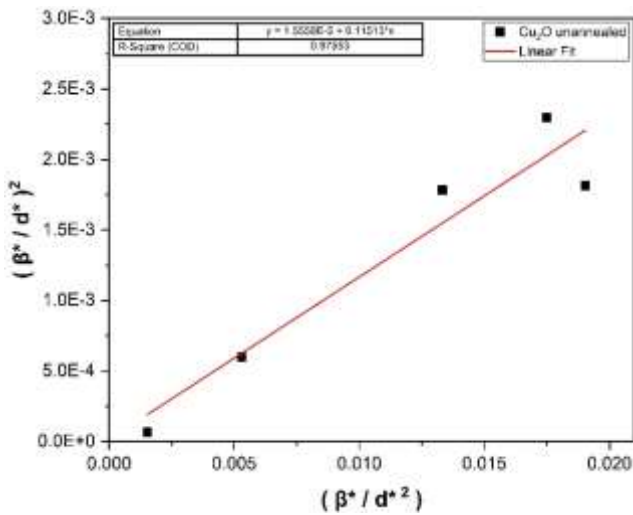
Table 5. result of Cu₂O NPs annealed at 500°C by Originpro

(h k l)	2θ 500°C	Area	FWHM	Height	β
(1 1 0)	29.78	50.235	0.1890	156.85	0.3203
(1 1 1)	36.56	1080.1	0.2808	2632.6	0.4103
(2 0 0)	42.39	349.25	0.4257	708.92	0.4927
(2 2 0)	62.51	323.47	0.6781	432.18	0.7485
(3 1 1)	73.46	175.41	0.5114	304.68	0.5757

3.1. Determination of crystallite size and the lattice strain

3.1.1. Halder-wagner method

After calculate the integral breadth of all peak for all five sample then we use equations $d^{*hkl} = 2\sin\theta / \lambda$ and $\beta^{*hkl} = \beta \cos \theta / \lambda$ where λ the wavelength of the X-ray (0.15046) and plot $(\frac{\beta^{*hkl}}{d^{*hkl}})^2$ against $(\frac{\beta^{*hkl}}{d^{*hkl}})^2$ then fitting the data by straight line to compare eq (1) by getting straight line equation to obtained crystallite size and the lattice strain. The outcomes are presented in **Tables (6)**.



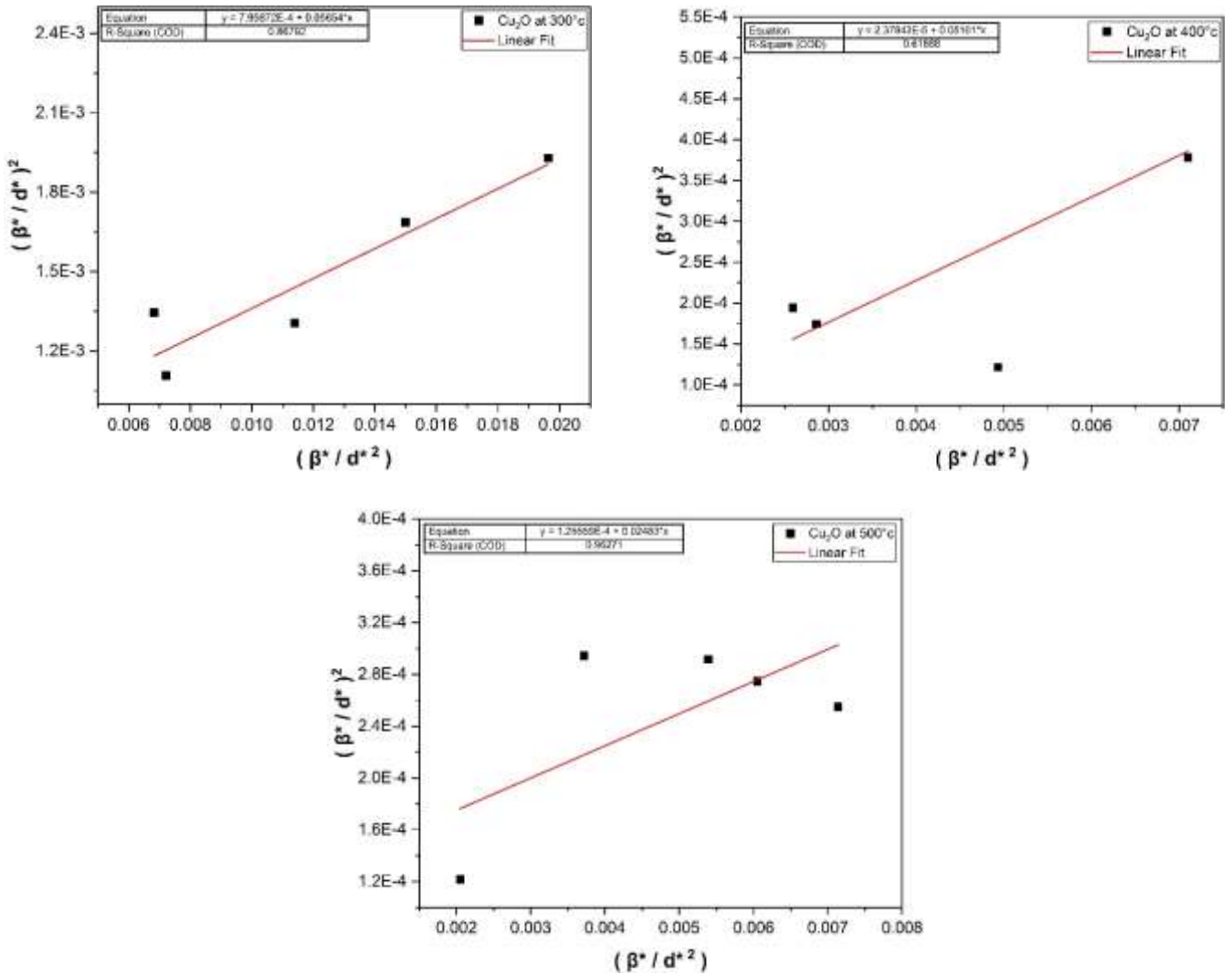


Figure 7. Halder-Wagner method for each sample respectively

Table 6. result of crystallite size and the lattice strain by Halder-Wagner method for all Cu₂O NPs sample

sample	D nm	ε strain
Cu ₂ O un-annealed	8.69	0.008
Cu ₂ O at 200°C	9.73	0.034
Cu ₂ O at 300°C	17.69	0.056
Cu ₂ O at 400°C	19.6	0.01
Cu ₂ O at 500°C	40.27	0.022

From the above five graphic figures, it is clear that by increasing the integrated width, it leads to an increase in the slope of the curve for each of the shapes, and this was actually found by calculating the particle size in this method. The annealing of Cu₂O nanoparticles shows that the higher the annealing temperature, the more highly oriented (111) planes could be formed with increasing annealing temperature.

i. Size-strain plot method

Each diffraction line's crystallite size is calculated using this method, and Equation (2) represents We can see in this technique an inverse relationship between crystal size and strain where $(\beta hkl / dhkl)^2$ represents the X axis, $(\beta hkl / d^2 hkl)^2$ represents the Y axis, and $d_{hkl}^2 B_{hkl} \cos \theta$ computed in

radians and utilizes a wavelength of X-ray equal to 0.15046 as shown in **Figure 8**. The outcomes were computed and are shown in **Table (7)**.

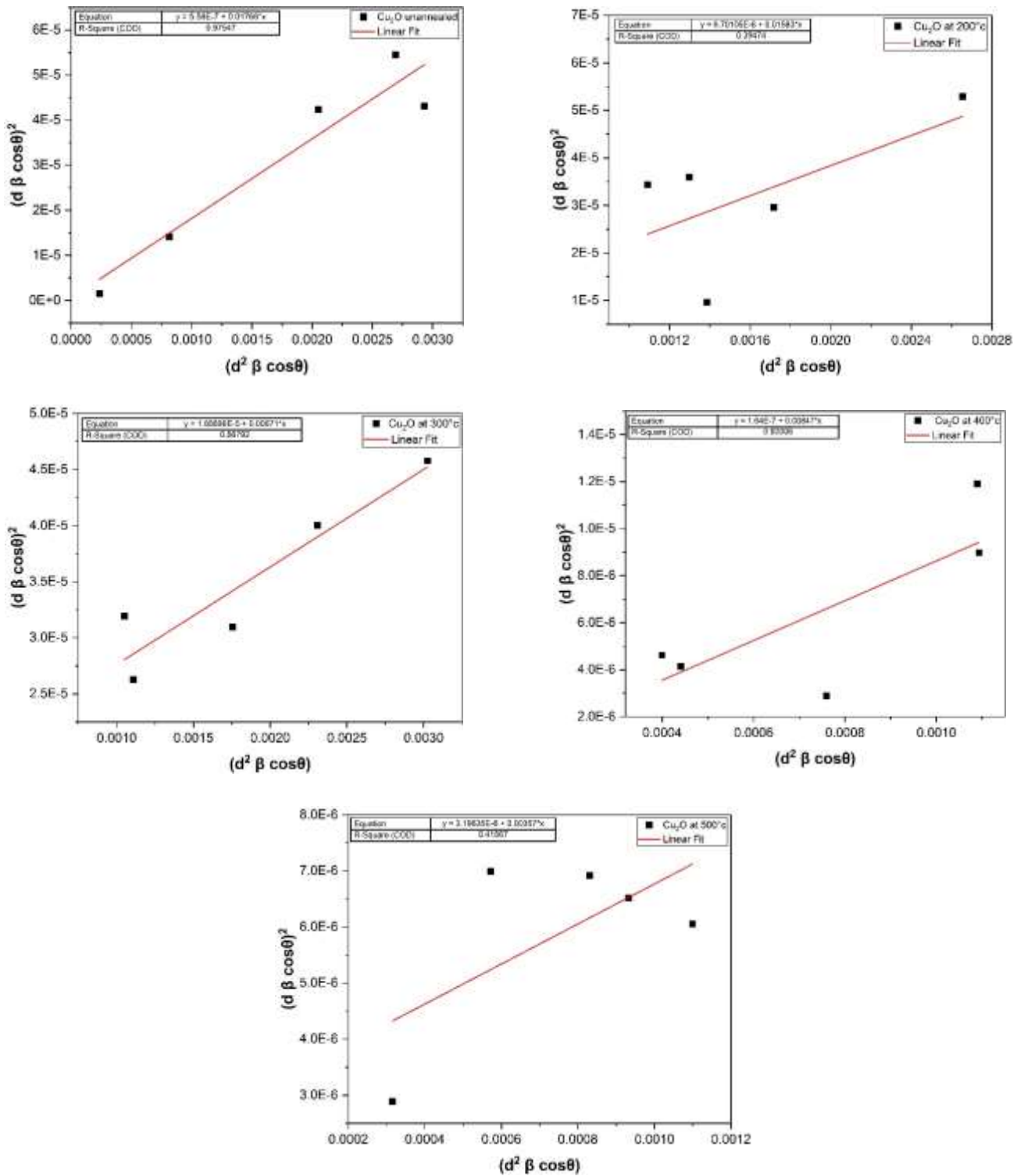


Figure 8. Size-strain plot method for each sample respectively

Table 7. Result of crystallite size and the lattice strain Size-strain plot method for all Cu₂O NPs sample

sample	D nm	strain
Cu ₂ O un-annealed	7.76	0.001
Cu ₂ O at 200°C	8.66	0.005
Cu ₂ O at 300°C	15.74	0.009
Cu ₂ O at 400°C	16.19	0.001
Cu ₂ O at 500°C	38.41	0.004

Also, in this method, the integral intensity change depends on the change in the temperature of each curve, and therefore there is a change in the value of the particle size, but here the effect of the shape coefficient value appears on the result.

From XRD we can work out the density of x-ray of the powders by using this equation [12]:

$$\rho = Z Mw / V N_{av} \tag{4}$$

Where ρ : the density (g/cm³), Mw: molar mass 143.091 (g/mol) for Cu₂O, Z: the number of atoms: unit cell volume (cm³), and N_{av}: Avogadro number (1/mol) [13]

To calculate volume for the cubic structure, lattice parameters can be calculated from:

$$1/d_{hkl}^2 = (h + k + l) 1/a^2 \tag{5}$$

Where $d_{hkl} = \lambda / (2 \sin \theta)$ d-spacing (Å) and h, k, and l are all integers, (hkl) is the lattice plane index, and a is lattice constants.

So the volume of Cu₂O is equal 76.96263 Å³ and density 6.03 (g/cm³)

The surface area can be determined by following equation [14]:

$$S.A = 6 * 10^3 / D \rho \tag{6}$$

And we can find dislocation density (δ) and number of unit cells (n) is calculated using the relation [15,16]:

$$\delta = 1/D^2 \tag{7}$$

$$n = \pi D^3 / 6 V \tag{8}$$

Their calculated values will be presented in **Table 8**.

Table 8. Shows lattice parameter, X-ray and dislocations density, surface area, and number of unit cells for all Cu₂O NPs sample

sample	Cu ₂ O un-annealed	Cu ₂ O at 200°C	Cu ₂ O at 300°C	Cu ₂ O at 400°C	Cu ₂ O at 500°C
S.A (m ² /g)	114.5	102.26	56.25	50.77	24.71
δ (1/m ²) *10 ¹⁶	1.32422	1.05627	0.319554	0.260308	0.0616647
n	4464.55	6266.96	37661.9	51225.59	444287

4. Conclusions

We can conclude from the results obtained for both methods (Halder-wagner and Size-strain plot) that increasing the temperature has a clear effect on the width of the middle of the intensity and thus an effect on increasing the particle size for both methods combined, but the increase in particle size in the T method is less due to the presence of a direct effect of the shape factor in the mathematical formula in this way. Also, there is a regular increase in the strain when observing the calculated values for this strain and for three temperatures in both methods. However, the high temperature and the last two values led to irregular strain (variation in strain values), which appears clearly in the results. It also appears that there is a clear decrease in the surface area and dislocation density with increasing temperatures due to the increase in particle size.

References

1. Nath, S. S.; Chakdar, D.; Gope, G.; Avasthi, D. K.; Characterization of CdS and ZnS quantum dots prepared via a chemical method on SBR latex. *Journal of nanotechnology online*, **2008**, *4*, 1-6.
2. Wang, X.; Zhuang, J.; Peng, Q.; Li, Y.; A general strategy for nanocrystal synthesis. *Nature*, **2005**, *437*(7055), 121-124.
3. Habubi, N. F.; Mishjil, K. A.; Rashid, H. G.; Rasheed, B. G.; Computation of Optical Energy Gap of Cu₂O Thin Film: Theoretical Estimation. *Iraqi Journal of Applied Physics Letters*, **2008**, *1*(1).
4. Xia, Y.; Yang, P.; Sun, Y.; Wu, Y.; Mayers, B.; Gates, B.; Yan, H.; One-dimensional nanostructures: synthesis, characterization, and applications. *Advanced materials*, **2003**, *15*(5), 353-389.
5. Ren, X.; Chen, D.; Tang, F.; Shape-controlled synthesis of copper colloids with a simple chemical route. *The Journal of Physical Chemistry B*, **2005**, *109*(33), 15803-15807.
6. Gholizadeh, A.; X-ray peak broadening analysis in LaMnO₃+ δ nano-particles with rhombohedral crystal structure. *Journal of Advanced Materials and Processing*, **2015**, *3*(3), 71-83.
7. Kamil, M. K.; Jasim, K. A.; Investigation the Crystalline Size and Strain of Perovskite (YBa₂Cu₃O₆) by variant method. *Test Engineering and Management*, **2020**, *83*, 8719-8723.
8. Kamil, M. K.; Jasim, K. A.; Calculating of crystalline size, strain and Degree of crystallinity of the compound (HgBa₂Ca₂Cu₃O₈+ σ) by different method. In *IOP Conference Series: Materials Science and Engineering*. **2020**, *928*(7), 072109 IOP Publishing.
9. Rabiei, M.; Palevicius, A.; Monshi, A.; Nasiri, S.; Vilkauskas, A.; Janusas, G.; Comparing methods for calculating nano crystal size of natural hydroxyapatite using X-ray diffraction. *Nanomaterials*, **2020**, *10*(9), 1627.
10. Xiong, L.; Xiao, H.; Chen, S.; Chen, Z.; Yi, X.; Wen, S.; Yu, H.; Fast and simplified synthesis of cuprous oxide nanoparticles: annealing studies and photocatalytic activity. *RSC Advances*, **2014**, *4*(107), 62115-62122.
11. Langford, J. I.; The use of the Voigt function in determining microstructural properties from diffraction data by means of pattern decomposition. *NIST Spec. Pub*, **1992**, *846*, 110-126.
12. Musa, K. H.; Investigating the Structural and Magnetic Properties of Nickel Oxide Nanoparticles Prepared by Precipitation Method. *Ibn Al-Haitham Journal For Pure and Applied Sciences*, **2022**, *35*(4).

13. Ramanathan, C.; Subramanian, S.; Valantina, R.; Structural and electronic properties of CuO, CuO₂ and Cu₂O Nanoclusters—a DFT approach. *Materials science*, **2015**, 21(2), 173-178.
14. Antony, J.; Nutting, J.; Baer, D. R.; Meyer, D.; Sharma, A.; Qiang, Y.; Size-dependent specific surface area of nanoporous film assembled by core-shell iron nanoclusters. *Journal of Nanomaterials*, **2006**, 12,23-34
15. Ajar, S. H.; Ahmad, E. Y.; Hussein, E. A.; Habib, A. A.; Study the Effect of Irradiation on Structural and Optical Properties of (CdO) Thin Films that Prepared by Spray Pyrolysis. *Ibn AL-Haitham Journal For Pure and Applied Science*, **2017**,28(2), 41- 51.
16. Singh, P.; Kumar, A.; Kaushal, A.; Kaur, D.; Pandey, A.; Goyal, R. N.; In situ high temperature XRD studies of ZnO nanopowder prepared via cost effective ultrasonic mist chemical vapour deposition. *Bulletin of Materials Science*, **2008**,31(3).